Case Studies in Construction Materials 18 (2023) e01918

Contents lists available at ScienceDirect

Case Studies in Construction Materials

journal homepage: www.elsevier.com/locate/cscm

Case study

Experimental investigation on expansion characteristics and strength of carbonating reactive magnesia solidified clay

Guoqian Hong [a], Wenhua Liu [a,*], Wugang Li [a], Pan Hu [b], Shiyi Huang [a], Gangqiang Kong [c]

[a] School of Environment and Civil Engineering, Jiangnan University, Wuxi 214122, China
[b] School of Engineering, Design and Built Environment, Western Sydney Univ., Penrith NSW 2751, Australia
[c] Key Laboratory of Ministry of Education for Geomechanics and Embankment Engineering, Hohai Univ., Nanjing 210098, Jiangsu, China

ARTICLE INFO

Keywords:
Carbonated reactive magnesia
Expansion stress
Volumetric expansion
Confining pressure
Clay

ABSTRACT

The carbonated reactive magnesia (CRM) method is superior in energy conservation, carbon capture, and rapid solidification in soil improvement. It has been revealed that CRM method could cause apparent volumetric expansion during carbonation, which may cause apparent compaction impact on the surrounding soils when used for soft foundation improvement. However, this expansion hasn't been discussed systematically. In this study, the evolutions of expansion stress (σ_{Ex}) and volumetric expansion (ΔV) during carbonation process were successfully monitored. Two factors, including reactive MgO content (C_m) and net confining pressure (P_{nc}), were investigated. The internal relations between σ_{Ex}, ΔV, and unconfined compressive strength (UCS) together with the influences of C_m and P_{nc} on them were discussed. Besides, the intrinsic mechanisms were discussed based on density variations, pore structures, and microstructures. According to the findings, σ_{Ex} and ΔV invariably exhibited a three-stage behavior consisting of stability-rapid increase-stability. By increasing C_m or P_{nc}, the σ_{Ex}, UCS, and density were all significantly increased, while the volume increment was obviously reduced. For the completely confined specimen, the σ_{Ex} and UCS were found to approach 3 MPa and 9 MPa, respectively. The increase in C_m promoted the crystallization of hydrated magnesium carbonates (HMCs), leading to lower porosity in solidified soils. Increasing P_{nc} also improved the crystallization of HMCs and modified pore structures, causing further increases in σ_{Ex} and UCS.

1. Introduction

In order to maintain the navigability of harbors and waterways and to protect the water ecosystems, vast sediments are dredged regularly [1]. These sediments widely exist around the world [2], especially in the Tai Lake basin of China [2–4]. They are always classified as soft soils with very poor engineering properties such as high compressibility, large void ratio and low structural strength [3]. Thus, these soft soils are usually unable to be used directly. Nevertheless, after suitable solidifications, they are potential to be utilized as backfilling, embankments, dikes, municipal waste barriers and et al. Well solidification techniques for soft soil stabilization benefit the environment, engineering and economy.

* Corresponding author.
E-mail addresses: 1713875958@qq.com (G. Hong), wenhualiu@jiangnan.edu.cn (W. Liu), lwgjn@jiangnan.edu.cn (W. Li), p.hu@westernsydney.edu.au (P. Hu), 1950837699@qq.com (S. Huang), gqkong1@163.com (G. Kong).

https://doi.org/10.1016/j.cscm.2023.e01918
Received 22 November 2022; Received in revised form 6 January 2023; Accepted 3 February 2023
Available online 4 February 2023

Nomenclature

C_m	Content of reactive magnesia (%).
w_0	Initial moisture content (%).
γ	Compactness (%).
σ_{Ex}	Expansion stress (kPa).
P_{nc}	Net confining pressure (kPa).
P_{ac}	Applied confining pressure (kPa).
P_c	Carbonation pressure (kPa).
q_u	Unconfined compressive strength (kPa).
ΔV	Volume variation after carbonation (cm^3).
$\Delta\rho$	Density variation after carbonation (g/cm^3).

Over the last few decades, Portland cement (PC) has been widely used in soft soil improvement [5,6]. While increasing concerns about energy conservation and carbon reduction have provoked greater interest in alternative greener cement binders [7]. The reactive magnesia, which is manufactured at a lower calcination temperature (<750 ℃) than PC (>1400 ℃) [8], has aroused wide interest in engineering constructions for its sustainability [9,10] in recent years. This material has been widely used as the primary binder or vital promotor in the fields of soil improvement [11–13], cement [14–16], and concrete [17] due to its efficient hydration ability and successive carbon-capture potential.

It is also utilized as the main raw material in the carbonated reactive magnesia (CRM) method, which is considered a substantial solidifying method in soft soil improvement [8,18,19]. The reactive MgO in this method can rapidly transform to brucite, as presented in Eq. (1), due to its high hydration efficiency. Under the appropriate conditions, the resulting brucite can absorb CO_2 and produce a variety of hydrated magnesium carbonates (HMCs), as shown in Eq. (2-5) [8]. These carbonate crystals can serve as skeletons, fill pores, and bond soil particles together, causing satisfactory solidification strength. The CRM method is superior for rapidly solidifying soils. It has been proven that CRM solidified samples can reach ideal strengths in few hours, comparable to PC solidified samples cured for 28 days [8]. CRM-treated soils also had sufficient resistance to sulfate attack to fully retain strength after immersion in Na_2SO_4 solution for 28 days [20]. Cai et al. [21] indicated that the soil strength of CRM-stabilized silt showed a slight decrease after several wetting-drying cycles, and the residual strength ratio was found to be 0.88 ~ 1.

$$MgO + H_2O \rightarrow Mg(OH)_2 \cdots \text{Brucite} \quad (1)$$

$$Mg(OH)_2 + CO_2 + 2H_2O \rightarrow MgCO_3 \cdot 3H_2O \cdots \text{Nesquehonite} \quad (2)$$

$$5Mg(OH)_2 + 4CO_2 + H_2O \rightarrow 4MgCO_3 \cdot Mg(OH)_2 \cdot 5H_2O \cdots \text{Dypingite} \quad (3)$$

$$5Mg(OH)_2 + 4CO_2 \rightarrow 4MgCO_3 \cdot Mg(OH)_2 \cdot 4H_2O \cdots \text{Hydromagnesite} \quad (4)$$

$$2Mg(OH)_2 + CO_2 + 2H_2O \rightarrow MgCO_3 \cdot Mg(OH)_2 \cdot 3H_2O \cdots \text{Artinite} \quad (5)$$

The CRM method has also been practically applied in the composite pipe pile [22] and soft foundation improvement [23]. Through using this method, the soil strength was significantly improved [22–25], and the soil permeability was apparently reduced [22]. However, due to the successive crystallizations of brucite and HMCs as presented in Eq. (1-5), it has been demonstrated by previous investigations that the CRM method can cause apparent volumetric expansion in treated specimens [13,24]. In practical engineering applications, the CRM process may cause apparent compaction impact on the surrounding soils, and the surrounding soils could also exert lateral confining pressure on the solidified soils. While to the best of the authors' knowledge, relevant expansion has not yet been systematically discussed. To fully comprehend and implement this carbonation method, it's necessary to clarify the magnitudes and the evolutions of expansion stress and the related volumetric expansion. Besides that, the horizontal compaction effect caused by this expansion on the surrounding soils was barely noticed, and the effect of lateral soil pressure on the CRM method's expansion also necessitates further investigation.

In the current study, clay specimens with 25% initial moisture content (w_0) and five different reactive magnesia contents (C_m) were prepared. A monitoring apparatus was specially prepared to record the evolutions of expansion stress and volumetric expansion. To further investigate the effect of lateral stress on the CRM method, six different net confining pressures (P_{nc}) were separately applied to the specimens with a C_m of 25%. After carbonation, properties including mass variations and unconfined compressive strength (UCS) were measured. The effects of C_m and P_{nc} were systematically discussed in relation to the results in expansion stress, volumetric expansion, UCS, mass, and density variation. The intrinsic influences of C_m and P_{nc} were revealed on a micromechanical scale via the SEM, XRD, and MIP tests.

2. Materials and methods

2.1. Materials

The utilized clay was collected from Baimao Bay near Tai Lake in Wuxi, China. Properties of this clayey soil detected according to the Chinese geotechnical testing standard GB/T 50123–2019 [26] are listed in Table 1. Tests to determine the properties of the soil were carried out after the soil had been sufficiently air-dried, crushed, and sieved ($\leq$ 2 mm). The Atterberg limits were determined by a fall cone test as per GB/T 50123–2019 [26], the soil was classified as lean clay (CL) according to GB/T 50145–2007 [27]. A Proctor compaction test was conducted to determine the maximum dry density ($\rho_{d,max}$) and optimum moisture content (w_{op}). The specific gravity (G_s) measurements were performed by a pycnometer method, and the soil pH was measured by a pH-meter.

The CO_2 gas used in the experimental study (99.9% in purity) was supplied by Wuxi Taihu gas CO., Ltd. The light-brown reactive magnesia powder was acquired from Yingkou, Liaoning, China, and the activity index (C_A) determined by Eq. (6) according to a hydration method [28] is 73.24%.

$$C_A = \frac{m_2 - m_1}{0.45 m_1} \tag{6}$$

where m_1 and m_2 represent the dry weight of MgO before and after hydration, respectively, and 0.45 is the molecular weight ratio of H_2O to MgO.

The grain sizes of clay and magnesia determined via a laser particle size analyzer (BT-2003) are presented in Fig. 1. Especially the detection of magnesia was performed by using absolute alcohol as the dispersant to prevent hydration. Table 2 presents the chemical compositions of these two solid materials detected by X-ray fluorescence (PANalytical Axios).

2.2. Specimen preparations

Specimen preparations started with pre-mixing a predetermined amount of powdered clay and reactive MgO. Subsequently, a certain amount of water was poured into the mixture, and the mixing procedure was continued. To avoid excessive evaporation, the entire mixture was sealed in a plastic bag. The specimens were then prepared by a compaction method using a mold which had an internal diameter of 39.1 mm and a height of 80 mm. All the specimens were compacted in 3 equal layers, and the total mass (M_t) of each specimen was determined by Eq. (7).

$$M_t = \rho_{d,\ max} \cdot \gamma \cdot V \cdot (1 + w_0) \tag{7}$$

where $\rho_{d,max}$ depicts the maximum dry density, V is the specimen volume, and γ presents the compactness of specimens. In this study, the γ values were controlled at 85%.

Specimens with an initial moisture content (w_0) of 25% (denoted as "W25″), and five reactive MgO content (C_m) including 15%, 20%, 25%, 30%, and 35% (denoted as "M15, M20, M25, M30, M35″, respectively) were prepared individually. Both w_0 and C_m were determined based on the dry weight of the soil. In order to ensure the test result reliability, three specimens were prepared for each test, and the average was reported.

2.3. Carbonation apparatus and methods

Fig. 2 illustrates the carbonation apparatus used in the experimental study. The confining cabin, the expansion stress monitor system, and the volume variation indicator are the main components of the apparatus. A pressure sensor (0.3 t) with an accuracy of 0.001 kN and a sealed water level indicator tube (50 ml) was used to monitor the change of expansion stress and volumetric expansion, respectively.

The prepared specimens were weighed before being placed at the base of the confining cabin. The bottom and top of the tested specimens were first covered with filter paper and then with a porous stone. The specimen with all attached objects were then covered with a latex film and a loading cap. After specimen preparation was completed, the cabin was installed, and the lifting platform was

Table 1
Basic properties of clay used in this study.

Index		Value
Plastic limit (w_P, %)		25.7
Liquid limit (w_L, %)		39.9
Plastic index (I_P, %)		14.2
Maximum dry density ($\rho_{d,max}$, g/cm^3)		1.76
Optimum moisture content (w_{op}, %)		17.6
Specific gravity (G_s)		2.71
pH		7.98
Grain size (μm)	D_{30}	9.4
	D_{60}	21.7

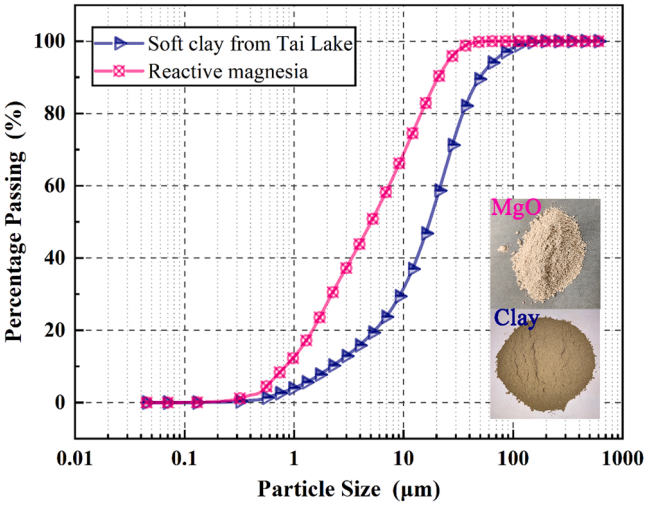

Fig. 1. Grain size distributions of used clay and reactive MgO.

Table 2
Chemical compositions of used clay and reactive MgO.

Oxide chemistry	Clay (%)	Reactive MgO (%)
MgO	5.22	88.33
SiO_2	61.62	6.49
CaO	2.68	1.94
Al_2O_3	17.99	1.66
Fe_2O_3	6.71	0.71
K_2O	2.11	0.07
Na_2O	1.46	–
P_2O_5	0.34	0.08
Other oxides	1.87	0.72

manually lifted to guarantee an accomplished vertical contact between the specimen, porous stone, loading cap, loading rod, and the pressure sensor. At the last stage, air-free water was infused by adjusting Valve 1 and Valve 2 to extrude the trapped air bubbles, fill the cabin and hold a moderate level in the indicator tube.

After installation, the water supply was stopped when it reached a sufficient level, and the confining pressure and carbonation pressure were applied separately. The applied confining pressure (P_{ac}) was transmitted from the water level indicator to the confining cabin and was loaded on the specimen. The applied confining pressure was determined by Eq. (8).

$$P_{ac} = P_{nc} + P_c \tag{8}$$

where the P_{nc} is arranged net confining pressure, and the P_c is carbonation pressure.

The applied CO_2 was transmitted through Valve 4 to the bottom of the specimen. Valve 3 was opened for 2 mins before each carbonation process to eliminate the trapped air by the CO_2. Afterward, Valve 3 was closed, and the specimen was subjected to accelerated carbonation. Owing to the adequate vertical contact, the vertical expansion stress (σ_{Ex}) can be monitored by the data acquisition system. Due to the hermetic condition, the volumetric changes of the specimens during the carbonation process were clearly measured by the change in the water level in the indicator tube. For all specimens, the σ_{Ex} was monitored per 10 s, and the volume variation was recorded per 15 mins. The accelerated carbonation period and the monitoring period were determined as 12 h, as it has been found that both the volume variation and σ_{Ex} tended to be stable after treating for 12 h in the preliminary experiments.

2.4. Experiment setups

As presented in Table 3, all specimens in this study were carbonated in a CO_2 environment with a gas pressure (inside the latex film) of 200 kPa, as has often been adopted in previous studies [13,29]. Besides, specimens with C_m ranging from 15% to 35% were separately carbonated with an identical confining pressure (P_{ac}) of 200 kPa (net confining pressure of 0 kPa) to investigate the effect of C_m.

In order to examine the effect of lateral soil stress at different depths on the CRM method, the effect of lateral confining pressure which can reflect the lateral soil stress in the field on the carbonation process has been investigated. In this study, six different net confining pressure (P_{nc}), including 0 kPa (P_{nc}-0), 50 kPa (P_{nc}-50), 100 kPa (P_{nc}-100), 200 kPa (P_{nc}-200), 300 kPa (P_{nc}-300) and

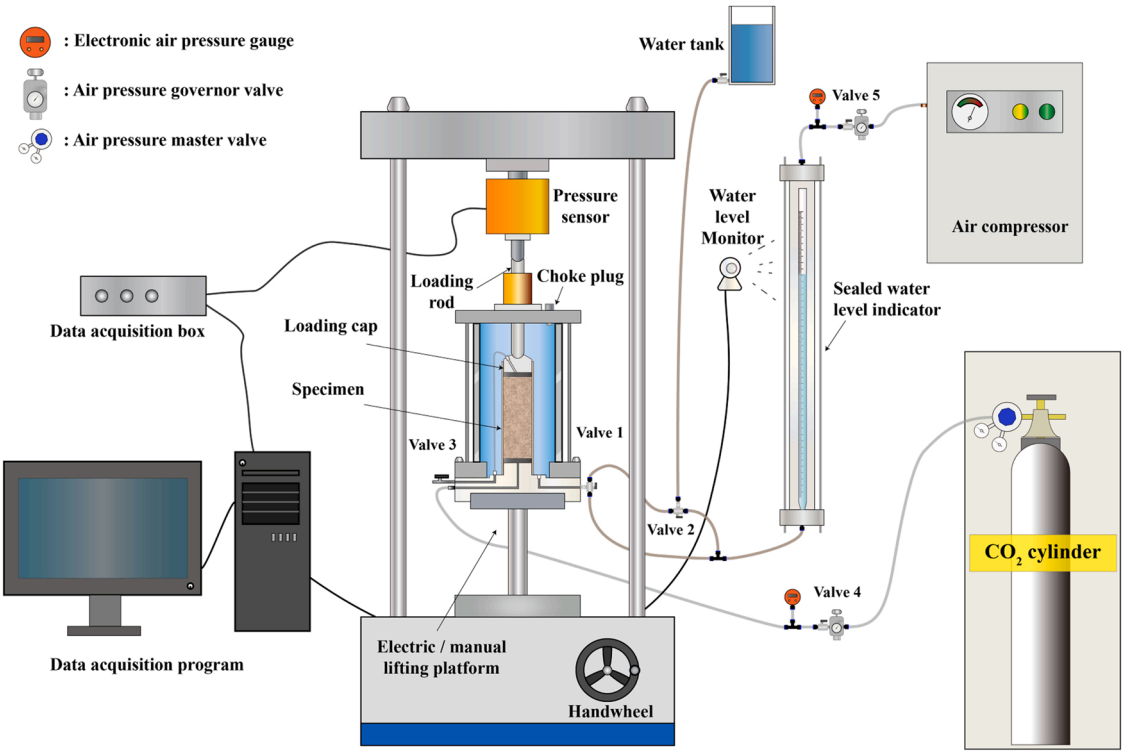

Fig. 2. Schematic diagram of the expansion stress and volume change monitoring system during the carbonation process.

Table 3
Pressure conditions and experiment setups.

P_{nc} (kPa)	Specimen	P_c (kPa)	P_{ac} (kPa)
0	W25M15,W25M20,W25M25 W25M30, W25M35	200	200
50	W25M25	200	250
100		200	300
200		200	400
300		200	500
CC		200	200

completely confined (P_{nc}-CC), were separately applied to specimen W25M25 to investigate the effect of lateral pressure on the carbonation process. Especially, to create a P_{nc}-CC condition, a set of special molds and two locking hoops were used to restrict specimens' horizontal expansion adequately.

2.5. Mechanical and microstructure test methods

After carbonation, the specimens were weighed, and the unconfined compressive strength (UCS) were determined with an automatic triaxial apparatus. Followed by the Chinese geotechnical testing standard GB/T 50123–2019 [26], the UCS tests were performed with a loading rate of 1 mm min^{-1}. Notably, the diameters of specimens (D_2) after carbonation were revised by Eq. (9) before every test.

$$D_2 = \sqrt{\frac{(\Delta V + V_s) \cdot 4}{H_s \cdot \pi}} \tag{9}$$

where the ΔV depicts the specimens' volume variation after carbonation, which is defined as positive in this paper. The V_s is the volume of specimen before carbonation (i.e., 96 cm^3). The H_s presents the height of the specimen after carbonation, which remains constant, i.e., 80 mm.

Following the UCS tests, the specimens were collected and adequately air-dried at 40 °C to prevent thermal decomposition of the HMCs [30]. The adequately air-dried specimens were selected for mercury intrusion porosimetry (MIP) tests, scanning electron

microscope (SEM) tests, and X-ray diffraction (XRD) tests. The specimens for MIP tests were carefully cut to be smaller than 15 mm × 15 mm × 15 mm. SEM test specimens were carefully exfoliated and attached to the observation platform, then the complete rough observing surface was gold-sprayed, and observed on a SEM (Zeiss Evo 18). The specimens for XRD tests were crushed and sieved ($\leq$ 0.075 mm), and then scanned from 5° to 65° (2-theta) at a rate of 5°/min.

3. Results and discussions

3.1. Expansion evolutions and unconfined compressive strength

Fig. 3 shows the appearance variations of carbonated specimens. As illustrated in Fig. 3, the smooth surface of specimens turned to be rough after carbonating treatment. Besides, the Pn-CC specimen barely varied in volume due to the complete lateral confinement, while the normal specimens presented apparent lateral expansion after carbonation.

To discuss the expansion phenomena more precisely, the evolutions of expansion during the carbonating process are expressed as the development of expansion stress (σ_{Ex}) and volumetric expansion (ΔV). Fig. 4a and Fig. 4b present the effects of C_m on σ_{Ex} and ΔV, respectively. As seen in Fig. 4a, the expansion stresses of all specimens barely increased during the first 2 h. With continued carbonation, expansion stresses showed a rapid increasing trend, and after approximately 8 h of carbonation, all specimens tended to be stable or slightly decreasing in expansion stress. The crystallization process can account for these phenomena. Crystals generated by the hydration and carbonation processes filled the pores in the soil during the early stage of carbonation; however, the amount of crystallization at this stage was insufficient to cause apparent expansion stress or volumetric expansion, resulting in a slight increase in σ_{Ex} during the first 2 h. The majority of the pores in soils were well filled by the successive carbonation process, and the remaining pores could not accommodate further HMC growth; thus, rapid increases for σ_{Ek} were noted in the carbonation process. However, as the carbon supply continued, the carbonation process almost completed, and the σ_{Ex} tended to be stable after 8 h of carbonation.

Additionally, as demonstrated by Fig. 4a, the increase in C_m could promote the expansion stress; in other words, the higher the C_m, the larger the σ_{Ex}. This behavior might be due to the fact that as the C_m increased, more HMCs were generated, which led to a significant increase in σ_{Ex}. As shown in Fig. 4b, during the carbonation process, the volume of all specimens barely increased, then increased rapidly after approximately 2 h, and finally tended to be stable, which was consistent with the overall trend of expansion stress. This result is also consistent with that found by Yi et al. [13], who found the volume of carbonated specimens barely changed when only carbonated for 1.5 h. It can be seen that the volume increment decreased with the increase in C_m, which was converse to the effect of C_m on σ_{Ex}. The main reason behind this might be the differences in the amount of HMCs crystals resulting from increased C_m. The increase in C_m led to the formation of a larger amount of HMCs; the soil particles were cemented to form a soil skeleton, resulting in an enhanced resistance of specimen to expansion deformation.

Fig. 5a and Fig. 5b depict the influences of P_{nc} on σ_{Ex} and ΔV, respectively. Fig. 5a demonstrated that higher P_{nc} caused greater increment in the σ_{Ex}. Particularly, the completely confined specimens exhibited a long-period steady increase in σ_{Ex}, with a maximum value of σ_{Ex} approaching to 3 MPa at 12 h. Besides, as presented in Fig. 5b, the increase in net confining pressure apparently reduced the total volume expansion. This demonstrated that the lateral confining pressure could apparently restrict the expansion of carbonated specimens and result in higher expansion stress and lower volume expansion. As presented in Fig. 5**a** and Fig. 5**b**, compared to the specimen under a P_{nc} of 0 kPa, a confining pressure of 50 kPa caused a slight increase in expansion stress while obvious reduction in the total volumetric expansion. This indicated that a small confining pressure could significantly reduce volume increase and slightly improve expansion stress.

Fig. 6a illustrates the relationships between unconfined compressive strength (UCS, q_u), expansion stress (σ_{Ex}), and reactive magnesia content (C_m), whereas Fig. 6b illustrates the relationship between UCS, expansion stress (σ_{Ex}) and net confining pressure (P_{nc}). The σ_{Ex} steadily increased with the increase in C_m or P_{nc}, according to Fig. 6a and Fig. 6b. Furthermore, the UCS increased exponentially with the increase of C_m, and it increased nearly linearly with the increase in P_{nc}. It can be referred to that both the increase in C_m and P_{nc} could improve the cementation ability of the CRM method, thus providing significant improvements in σ_{Ex} and UCS. The increase in C_m might improve the amount and the morphologies of HMCs crystals, which showed improvement in the expansion potential and cementation ability of solidified soils. As the expansion potential improved, the expansion stress obviously

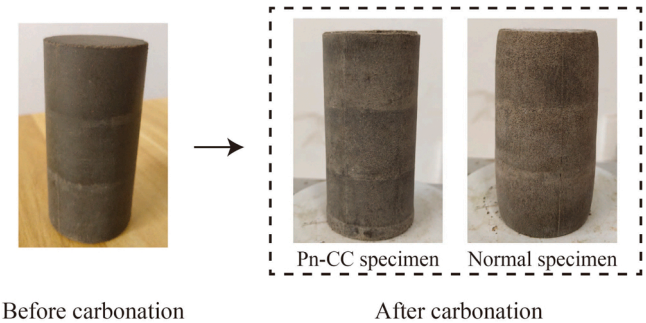

Fig. 3. Appearance variations of carbonated specimens after carbonation treatment.

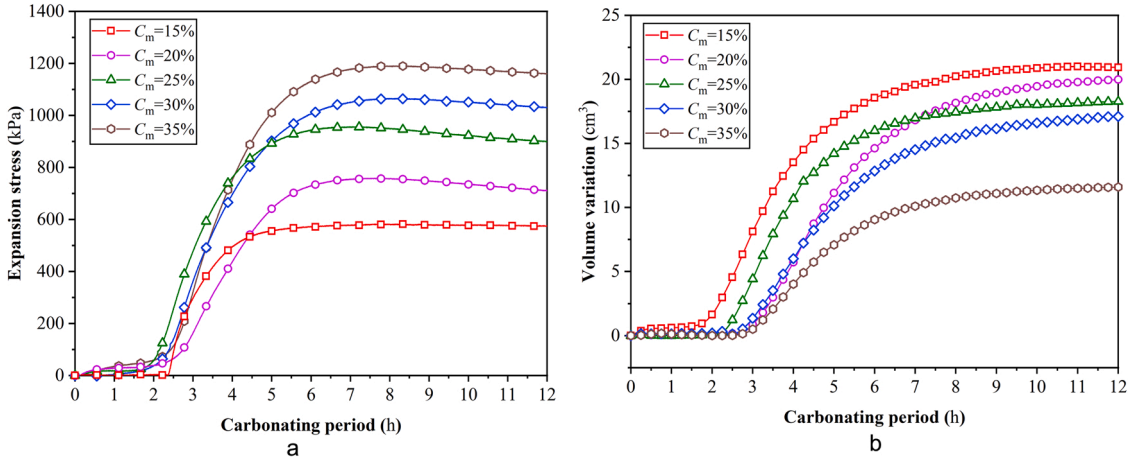

Fig. 4. a Effect of C_m on the expansion stress, Effect of C_m on the volumetric expansion.

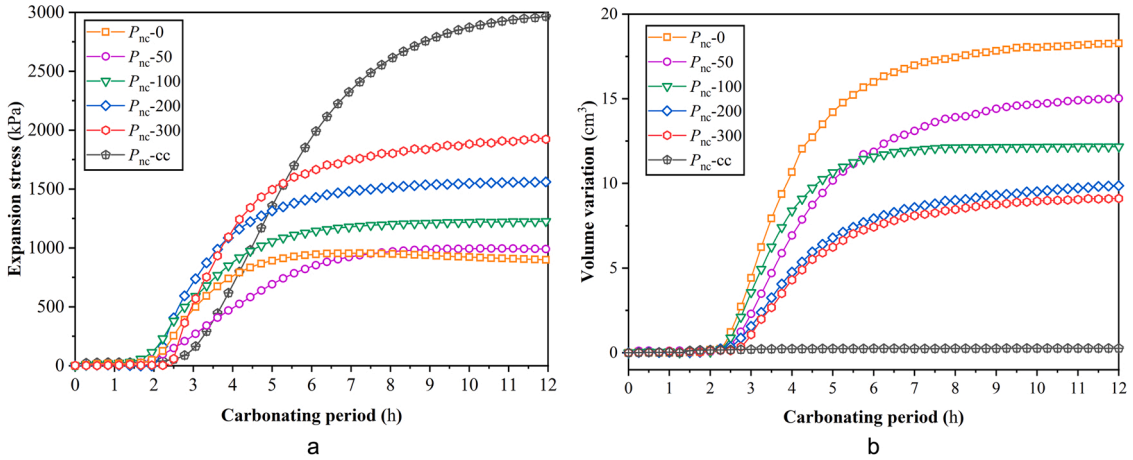

Fig. 5. a Effect of P_{nc} on the expansion stress, Effect of P_{nc} on volumetric expansion.

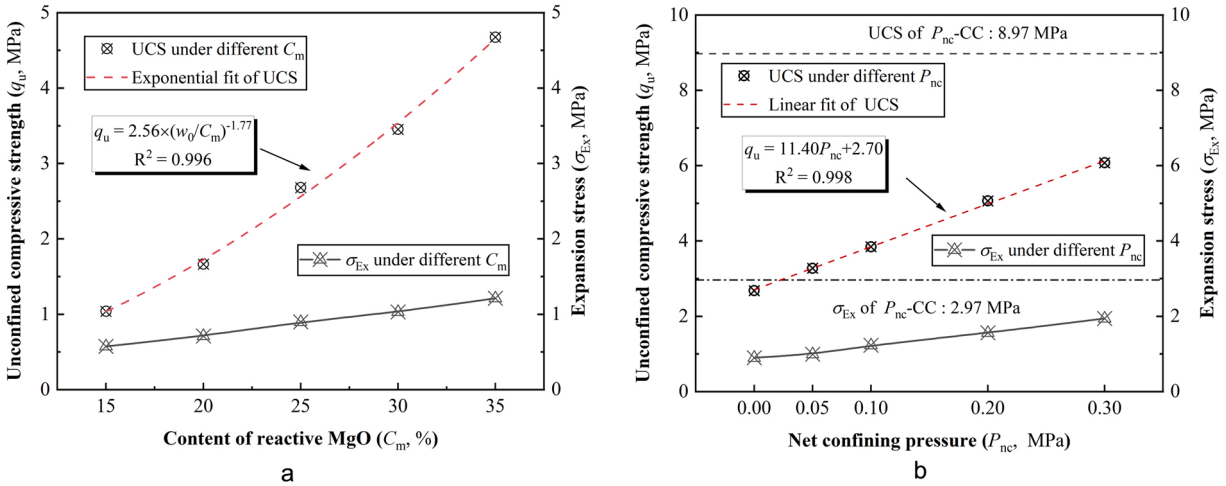

Fig. 6. a Relation between UCS, $\sigma_{Ex,}$ and C_m, Relation between UCS, $\sigma_{Ex,}$ and P_{nc}.

improved. Also, as the cementation ability improved, denser cementation structures occurred in the treated soils; thus, the UCS and σ_{Ex} increased. While the increase in P_{nc} might restrict the expansion of specimens which caused the generation of denser structures in soils and resulted in higher σ_{Ex} and q_u. Especially for the completely confined specimen, extremely high expansion stress and UCS occurred under this condition. This could be attributed to the completely confined state, which strictly limited the volumetric expansion so that the formation of crystals during processing could only form cementation; however, it did not cause expansion damage between soil particles, which ultimately led to a long-term steady increase in expansion stress and extremely high strength.

The aforementioned exponential relation between UCS (q_u) and w_0/C_m is expressed by a modified Abrams' law as presented in Eq. (10), which was utilized to present the UCS of PC-solidified soft soil [31]. The obtained relation of q_u and w_0/C_m in this study is also well expressed based on the modified Abrams' law, as shown in Eq. (11). The relation between q_u and P_{nc} is well expressed by a linear fit as shown in Eq. (12).

$$q_u = A \times (w_0/C_m)^B \tag{10}$$

where A and B are dimensionless constants effected by factors like carbonating time, etc.

$$q_u = 2.56 \times (w_0/C_m)^{-1.77} \cdots \ R^2 = 0.996 \tag{11}$$

$$q_u = 11.40 \times P_{nc} + 2.70 \cdots \ R^2 = 0.998 \tag{12}$$

Best fits based on the data were performed to elucidate the numerical relationships between the σ_{Ex}, ΔV, and UCS. The results are presented in Fig. 7. The relation between the expansion stress (σ_{Ex}) and the volume increment (ΔV) is shown in Fig. 7a. The σ_{Ex} decreased gradually as the ΔV increased. It might be inferred that as C_m or P_{nc} increased, the ΔV was decreased, and both the cementation ability and expansion potential of CRM were improved, resulting in the apparent increase in σ_{Ex}. To clarify the relation between σ_{Ex} and ΔV, a linear fit of the obtained results is conducted as presented in Eq. (13).

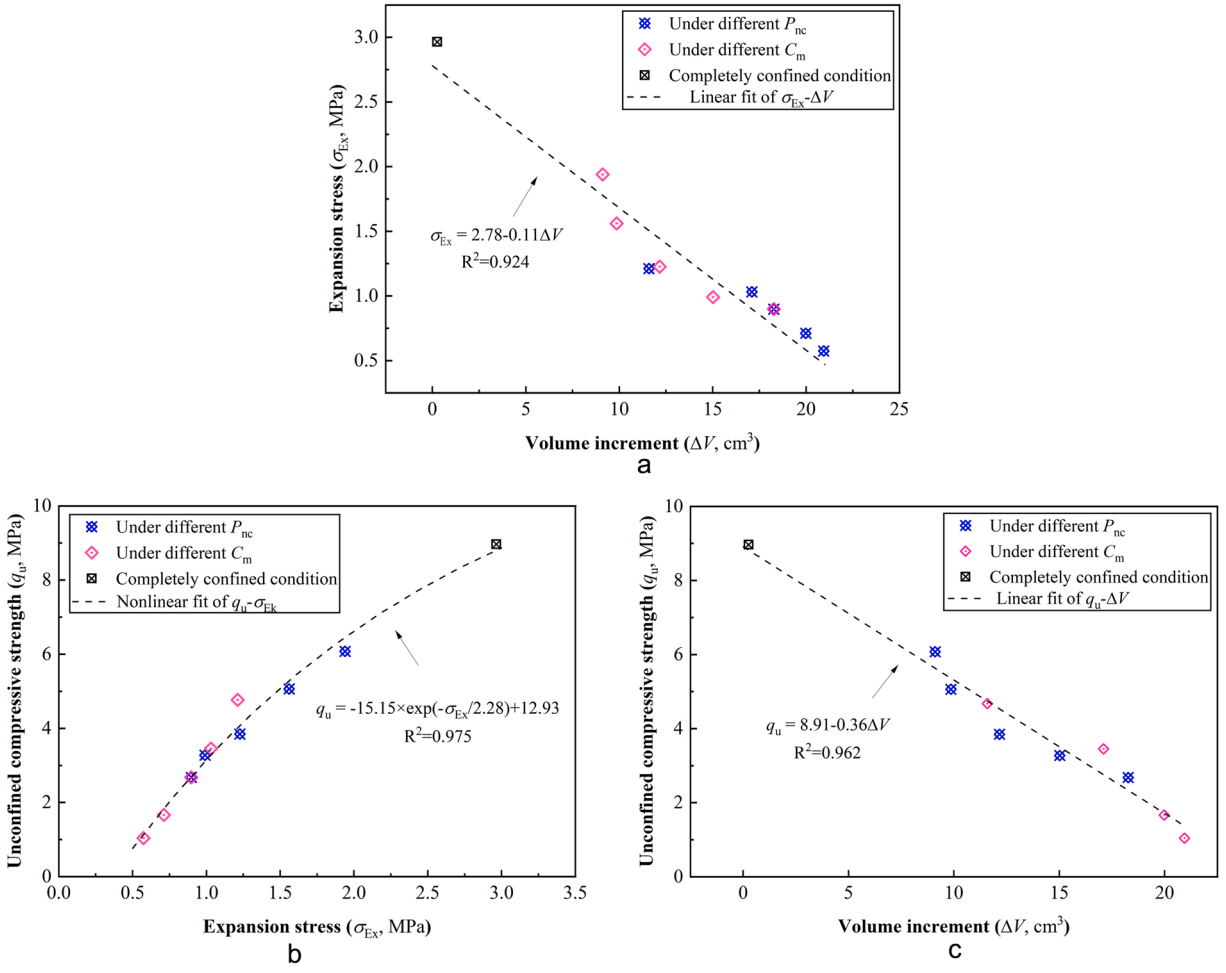

Fig. 7. **a** Relation between σ_{Ex} and ΔV, **b** Relation between UCS and σ_{Ex}, **c** Relation between UCS and ΔV.

$$\sigma_{Ex} = 2.78 - 0.11 \times \Delta V \cdots R^2 = 0.924 \quad (13)$$

The relation between UCS and expansion stress is shown in Fig. 7b. The UCS suffers a nonlinear increase with the increase of expansion stress within the investigated ranges of C_m, and this relation can be expressed by Eq. (14).

$$q_u = -15.15 \times e^{(-\sigma_{Ex}/2.28)} + 12.93 \cdots R^2 = 0.975 \quad (14)$$

The relation between UCS and volume expansion is shown in Fig. 7c. As the volume increment diminishes, the UCS gradually rises, and this relationship is expressed by a linear fit, as shown in Eq. (15).

$$q_u = 8.91 - 0.36 \times \Delta V \cdots R^2 = 0.962 \quad (15)$$

3.2. Volume, mass, and density

After the accelerated carbonation process, specimens all experienced apparent increases in both mass and volume, which were caused by the crystallization of HMCs [13,24]. The mass increment and volume increment under different C_m or P_{nc} are depicted in Fig. 8a and Fig. 8b, respectively. As seen in Fig. 8a, the mass increment rose gradually as C_m rose; this phenomenon might be explained by the fact that increased C_m enhanced specimens' capacity to trap carbon and, as a result, increased the quantity of HMCs. The large amount of HMCs led to better cementation between soil particles and enhanced the resistance of specimen to expansion deformation, resulting in a decrease in the volume increment with the increase in C_m, as shown in Fig. 8a. While referring to Fig. 8b, with the increase of P_{nc}, the volume increment first decreased rapidly and then tended to be stable under relatively high confining pressures. Besides, as the net confining pressure increased, the mass increment increased and then tended to reach a plateau. These phenomena demonstrated that the lateral confining pressure could restrict the volumetric expansion, which was also beneficial for mass increment. With the increase in confining pressure, the mass increment increased, and the volume increment decreased, which was extremely apparent under the relatively low confining pressure ($\leq$ 100 kPa). While under relatively high P_{nc} (i.e., 200kPa and 300kPa), only slight variation of the volume or mass increment was observed. It could be concluded that under the relatively high P_{nc} conditions, the large pores between soil particles were almost thoroughly filled with the generated crystals of HMCs and brucite, while the volumetric expansion was strictly limited under these conditions. Therefore, further increment in confining pressure might have an insignificant effect on reducing the volumetric expansions or promoting the mass increment.

Based on the test results in Fig. 8, the carbonation-induced density variation ($\Delta\rho$) is calculated by Eq. (16).

$$\Delta\rho = \frac{m_c}{\Delta V + V_s} - \frac{m_s}{V_s} \quad (16)$$

where m_s and m_c are the specimen's mass before and after carbonation, respectively, and ΔV is the specimens' volume variation after carbonation. V_s is the volume of the specimen before carbonation (i.e., 96 cm^3).

The changes of $\Delta\rho$ with C_m and P_{nc} are shown in Fig. 9a and Fig. 9b, respectively. The accelerated carbonation process resulted in a slight decrease in density in most specimens, which might be mainly due to the volumetric expansion caused by the crystallization of HMCs. However, as either C_m or P_{nc} increased, the density raised, especially for specimens under relatively higher confining pressure (i.e., specimens W25Pnc-200, W25Pnc-300, and W25Pnc-CC), their densities were even slightly increased after the carbonation. This could mainly be explained by the reduction in volumetric expansion and the increase in mass increment resulting from the increase in C_m or P_{nc} that finally led to the increase in density. Besides, as depicted in Fig. 9a, $\Delta\rho$ increased exponentially with the increase of C_m.

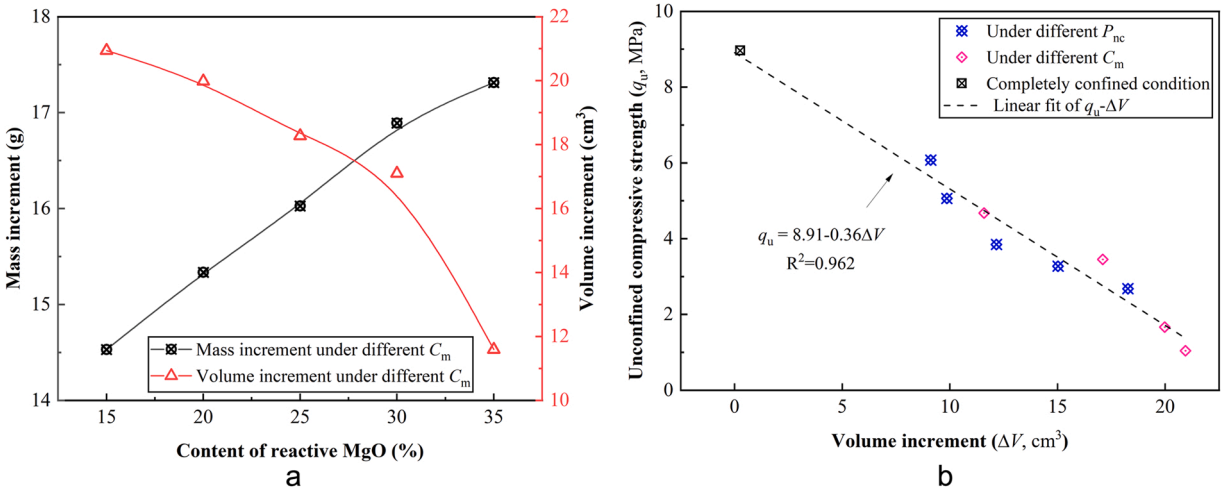

Fig. 8. a Mass and volume increment under different C_m, Mass and volume increment under different P_{nc}.

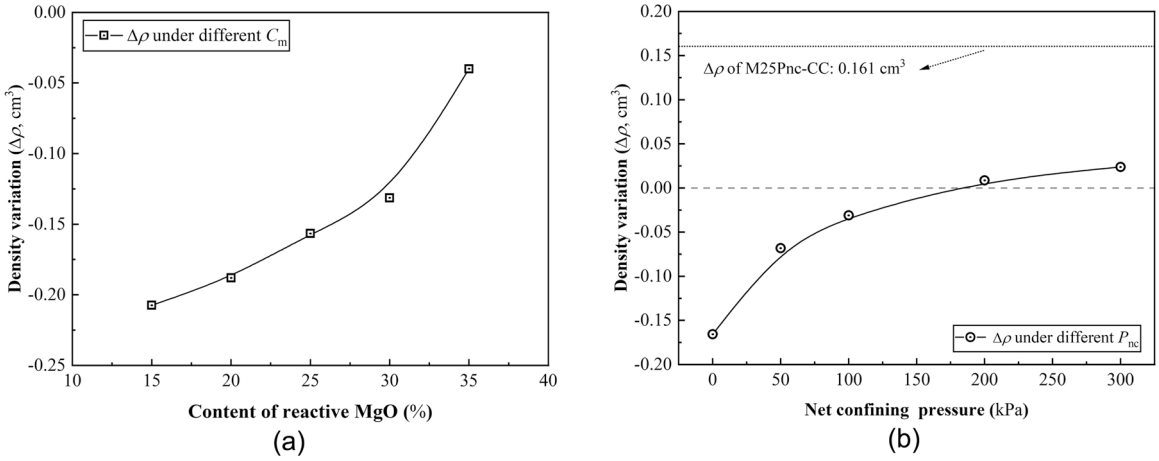

Fig. 9. a Relation between density variation and C_m, Relation between density variation and P_{nc}.

This indicated that the density of solidified soils could be clearly improved by increasing the reactive magnesia content. A small net confining pressure could improve the density of solidified soils, as depicted in Fig. 9b. With the successive increase in net confining pressure, the density increment gradually reached a plateau because the volume increment and the mass increment were both varied slightly under high confining pressure conditions, as shown in Fig. 8b.

Fig. 10a depicts the relation between expansion stress and density variation under different C_m or P_{nc}, while Fig. 10b presents the relation between UCS and density variation under different C_m or P_{nc}. It was seen that both σ_{Ex} and UCS increased markedly as the density increased, and both expressed in exponential relationships, as shown in Eq. (17) and Eq (18).

$$\sigma_{Ex} = 1.62 \times e^{(\Delta\rho/0.25)} - 0.06 \cdots R^2 = 0.966 \tag{17}$$

$$q_u = 15.19 \times e^{(\Delta\rho/0.74)} - 9.96 \cdots R^2 = 0.952 \tag{18}$$

The increase in density indicated that denser structures were formed in soils, which led to a significant improvement in UCS and σ_{Ex}, and might be the intrinsic mechanism of the improvement in UCS and σ_{Ex} by increasing C_m or P_{nc}. Furthermore, as discussed above, the cementation ability of CRM was well improved by the increase of C_m, and this led to the increase in density, which was also considered for the increase in σ_{Ex} and UCS of solidified specimens. While as the P_{nc} increased, the specimens experienced an increasing inhibition in volumetric expansion. Thus, denser structures were formed in soils, leading to increase in σ_{Ex} and UCS. As a result, both the σ_{Ex} and UCS increased with the increase of density variation.

3.3. Pore structures

M15W25, M25W25P_{nc}-0, and M25W25P_{nc}-100 specimens were chosen for the mercury intrusion porosimetry (MIP) tests to

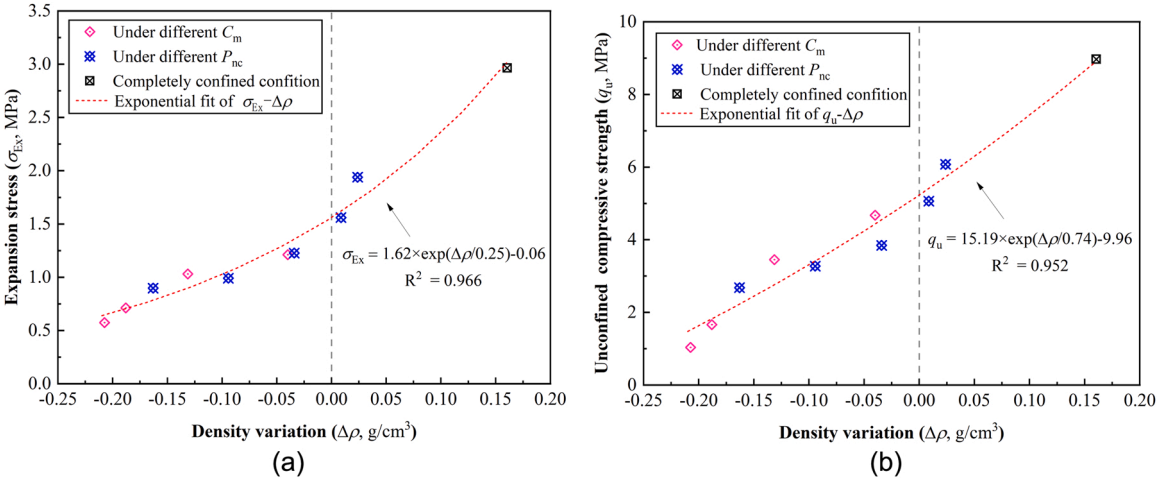

Fig. 10. **a** Relation between σ_{Ex} and Δρ, **b** Relation between UCS and Δρ.

investigate the intrinsic distinctions in pore structures. The cumulative pore volume and pore size distribution curves are shown in Fig. 11a and Fig. 11b, respectively.

In Fig. 11a, the chosen specimens demonstrated similar relation between cumulative pore volume and pore diameter. It could be observed that the porosity of specimen M15P_{nc}-0 (34.01%) was apparently higher than the other two specimens (31.07% for M25W25P_{nc}-0% and 30.53% for M25W25P_{nc}-100, respectively); this could be explained by the increase in C_m that promoted the crystallization of HMCs, which filled the pores in soils better and resulted in an apparent reduction in porosity.

The pore-size distribution curves depicted in Fig. 11b were obtained based on the ratio of the cumulative derivatives of pore volumes and the derivatives of pore diameter. In previous studies, the pore size of solidified soils was usually divided into four stages [6], which were intra-aggregate pores (<0.01 μm), small inter-aggregate pores (0.01–1 μm), large inter-aggregate pores (1–10 μm), and macropores (>10 μm), respectively. According to Fig. 11b, three peaks at about 0.1 μm, 3 μm, and 7 μm existed in all the specimens. The M15P_{nc}-0 specimen had the highest porosity due to its exceptionally high peak, which was present at about 0.1 μm and 7 μm. Also, it could be inferred that the increase in C_m could modify the pore structures in soils by reducing the large and small inter-aggregate pores. When comparing the M25P_{nc}-0 and M25P_{nc}-100, apparent differences in peaks occurred at the pore diameter of about 0.1 μm and 7 μm. The M25P_{nc}-100 had lower large inter-aggregate pores while higher small inter-aggregate pores, which is reflected by the increase in P_{nc}, strengthening the connections between soil particles and facilitating the large inter-aggregate pores to convert to small inter-aggregate pores. This ultimately led to the lower large inter-aggregate pores while higher small inter-aggregate pores.

3.4. Microstructures

The scanning electron microscope (SEM) tests and the x-ray diffraction (XRD) tests were conducted on the chosen specimens to further investigate the intrinsic effects of C_m and P_{nc}.

The images from SEM with a magnification of 5000 times are illustrated in Fig. 12. The solid particles, including clay (flake-like), brucite (porous flocculation blobs [32]), and various HMCs were clearly seen in these images. The HMCs usually occur in solidified soils in the forms of the rosette flaky dypingite/hydromagnesite (D/H) and the elongated-prismatic or rod-like nesquehonite (N), as stated by previous research [13,15,33,34]. The pores in specimen M15Pnc-0 were well filled by massive sprawling petal-like D/H crystals, as seen in Fig. 12**a**. The results above indicated that this specimen had a considerably higher volumetric expansion and relatively lower expansion stress and UCS. This might be caused by the crystallization of HMCs that formed not only cementation but also expansion damage in soils. The cementation and the expansion stress could be relatively weaker due to the deficiency of reactive MgO, resulting in relatively looser structures in soils. While as presented in Fig. 12b and Fig. 12c, the rod-like N, which was typically regarded as more advantageous than D/H in terms of strength enhancement, was generally observed with the increase in C_m. In these images, the observed N filled the pores and generated dense soil structures. In addition, the N crystals of the specimen presented in Fig. 12f were more angular and thicker than the others. They were embedded in the soil particles and formed ideal cementations, thus leading to higher expansion stress and solidification strength. Furthermore, as shown in Figs. 12b, 12d, and 12e, the crystal N tended to agglomerate with the soil particles, modifying the granular state of clay particles and resulting in an apparent improvement in strength. It should be noted that compared to the D/H crystals, N crystals were more frequently observed through the SEM. And this might be caused by the continuous carbonation that significantly reduced the pH, and the decreasing pH was usually thought to be conductive to the crystallization of N [35].

The results of XRD for different C_m and different P_{nc} are illustrated in Fig. 13. Apart from the widely existed peaks of Quartz (e.g., 4.24 Å, 4.02 Å, 3.34 Å, 2.45 Å), which was one of the main mineral compositions (SiO_2) of clay, peaks of the brucite and various HMCs were also detected. The detected brucite may be the remainder of the uncarbonated hydrated reactive magnesia. Moreover, the detected peaks of brucite were relatively weak, indicating that most brucites converted successfully into the HMCs in the carbonation process. Besides, higher peaks of various HMCs crystals, including D, H, N, and A (artinite), were frequently observed. Among all the HMCs crystals, the N is usually considered vital in improving the solidification strength [24]. Consistent with the SEM results, the N exhibited much higher peaks than the other HMCs, indicating that N was the dominant HMCs in the solidified specimens. With comparisons of the N-peaks at a 2θ of about 13.699° (6.47 Å), the intensity of N increased with the increase in C_m or P_{nc}. This behavior indicated that the increase in C_m or P_{nc} could facilitate the crystallization of N, attributing to the higher strength and expansion stress as the C_m or P_{nc} increases.

4. Conclusion

The evolutions of expansion stress (σ_{Ex}) and volumetric expansion (ΔV) of carbonated reactive magnesia (CRM) solidified clay were successfully monitored in the current study. The effects of reactive magnesia content (C_m) and net confining pressure (P_{nc}) on the σ_{Ex}, ΔV, and UCS of the solidified specimens were investigated. Besides, tests including the mercury intrusion porosimetry (MIP), scanning electron microscope (SEM), and X-ray diffraction (XRD) were conducted to further investigate the intrinsic effects of C_m and P_{nc}. Based on the obtained results, the following conclusions can be drawn:

1. The CRM method could cause high expansion stress and volumetric expansion, especially for the completely confined specimen, the expansion stress could even reach approximately 3 MPa. The σ_{Ex} and ΔV significantly increased after carbonating for about 2 h and finally tended to be stable after 8 h. Moreover, they were apparently influenced by the C_m and P_{nc}. In summary, the higher the P_{nc} or C_m, the higher the σ_{Ex}. While variations in ΔV were exactly the opposite, the higher the P_{nc} or C_m, the lower the ΔV.

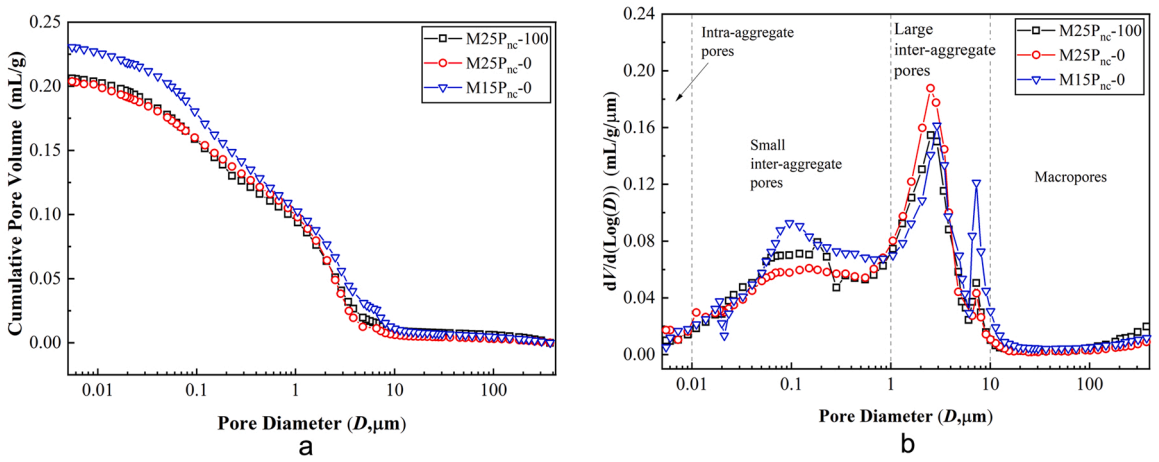

Fig. 11. **a** Cumulative pore volume curves, **b** Pore size distribution curves.

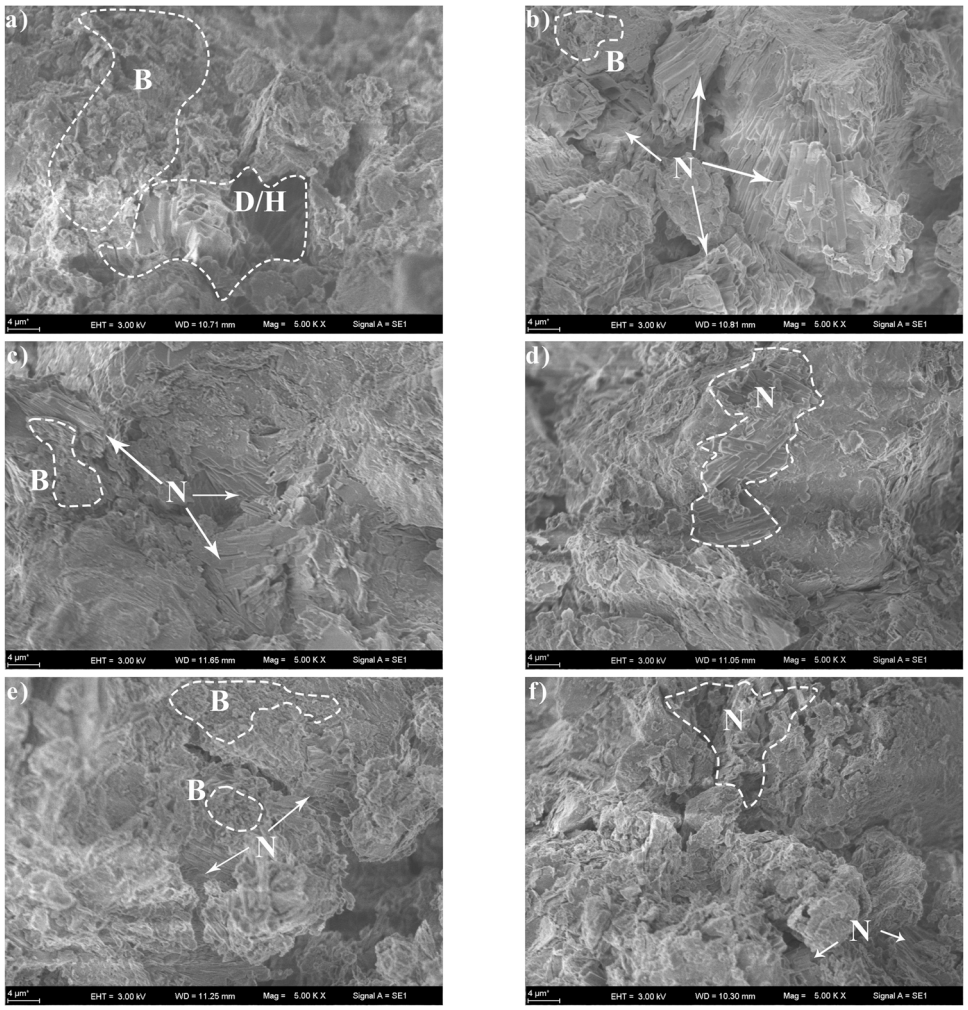

Fig. 12. SEM images of a) M15P_{nc}-0, b) M25P_{nc}-0, c) M35P_{nc}-0, d) M25P_{nc}-100, e) M25P_{nc}-300 and f) M25P_{nc}-CC.

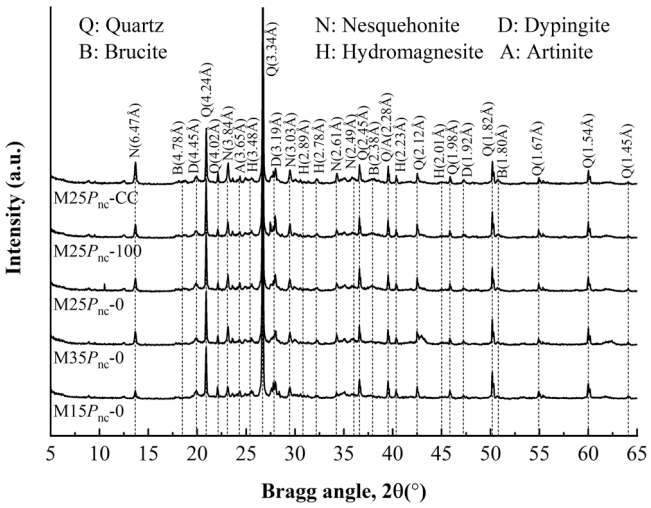

Fig. 13. X-ray diffractograms of specimens M15P_{nc}-0, M25P_{nc}-0, M35P_{nc}-0, M25P_{nc}-100, and M25P_{nc}-CC.

2. The UCS of solidified specimens had an increment trend along with the increase in σ_{Ex} or the decrease in ΔV, and especially the completely confined specimens had extremely high UCS of 9 MPa. The main reason behind this was the density variations caused by carbonation. In general, apart from the specimens under high confining pressure and the completely confined cases, the density slightly decreased after carbonation. At the same time, the increase in C_m or P_{nc} promoted the final density of the solidified specimens. Moreover, increase in the final density caused the σ_{Ex}, and UCS to be increased.
3. The increase of C_m could significantly reduce the porosity, and the increase in P_{nc} might facilitate the large inter-aggregate pores to transform into the small inter-aggregate pores leading to the increase in σ_{Ex} and cementation strength. Plentiful hydrated magnesium carbonate crystals (HMCs) and minor brucite were detected by the SEM and XRD tests. The nesquehonite crystals was the dominate HMCs which can agglomerate with the extremely fine soil particles to form coarse granules and improve the strength of CRM solidified specimens.
4. The special expansion effect of the CRM method has the potential to improve the interaction between treated soils and surrounding soils. The lateral confining pressure can improve the expansion stress and solidification strength, indicating that the lateral soil stress exerted by the surrounding soils can also improve the solidification efficiency. Further investigations on the application of in-situ carbonation technologies are needed in future, and this would be of great interest and significance.

Declaration of Competing Interest

The authors declare that no known competing financial interests or personal relationships exist that could influence the work reported in this paper.

Data Availability

Data will be made available on request.

Acknowledgement

The authors gratefully acknowledge the National Natural Science Foundation of China [grant 51709129, 52009049] and the Key Laboratory of the Ministry of Education for Geomechanics and Embankment Engineering, Hohai University [grant No.2020004].

References

[1] Y. Huang, W. Zhu, X. Qian, N. Zhang, X. Zhou, Change of mechanical behavior between solidified and remolded solidified dredged materials, Eng. Geol. 119 (3–4) (2011) 112–119.
[2] X. Zhang, X. Fang, J. Liu, M. Wang, C. Shen, K. Long, Durability of solidified sludge with composite rapid soil stabilizer under wetting–drying cycles, Case Stud. Constr. Mater. 17 (2022).
[3] J. Xia, G. Huang, S. Yan, Behaviour and engineering implications of recent floodplain soft soil along lower reaches of the Yangtze River in Western Nanjing, China, Eng. Geol. 87 (1–2) (2006) 48–59.
[4] Y. Huang, C. Dong, C. Zhang, K. Xu, A dredged material solidification treatment for fill soils in East China: a case history, Mar. Georesources Geotechnol. 35 (6) (2016) 865–872.
[5] R. Saadeldin, S. Siddiqua, Geotechnical characterization of a clay–cement mix, Bull. Eng. Geol. Environ. 72 (2013) 601–608.
[6] S. Horpibulsuk, R. Rachan, A. Chinkulkijniwat, Y. Raksachon, A. Suddeepong, Analysis of strength development in cement-stabilized silty clay from microstructural considerations, Constr. Build. Mater. 24 (10) (2010) 2011–2021.

[7] W. Yang, F. Zhou, R. Zhu, Z. Song, S. Hua, Y. Ma, Strength performance of mucky silty clay modified using early-age fly ash-based curing agent, Case Stud. Constr. Mater. 17 (2022).
[8] Y. Yi, M. Liska, C. Unluer, A. Al-Tabbaa, Carbonating magnesia for soil stabilization, Can. Geotech. J. 50 (8) (2013) 899–905.
[9] S. Ruan, C. Unluer, Comparative life cycle assessment of reactive MgO and Portland cement production, J. Clean. Prod. 137 (2016) 258–273.
[10] S. Ruan, C. Unluer, Influence of supplementary cementitious materials on the performance and environmental impacts of reactive magnesia cement concrete, J. Clean. Prod. 159 (2017) 62–73.
[11] G. Cai, S. Liu, Compaction and mechanical characteristics and stabilization mechanism of carbonated reactive MgO-stabilized silt, KSCE J. Civ. Eng. 21 (7) (2017) 2641–2654.
[12] D. Wang, M. Benzerzour, X. Hu, B. Huang, Z. Chen, X. Xu, Strength, permeability, and micromechanisms of industrial residue magnesium oxychloride cement solidified slurry, Int. J. Geomech. 20 (7) (2020).
[13] Y. Yi, K. Lu, S. Liu, A. Al-Tabbaa, Property changes of reactive magnesia–stabilized soil subjected to forced carbonation, Can. Geotech. J. 53 (2) (2016) 314–325.
[14] Y. Yang, S. Ruan, S. Wu, J. Chu, C. Unluer, H. Liu, L. Cheng, Biocarbonation of reactive magnesia for soil improvement, Acta Geotech. 16 (2021) (2021) 1113–1125.
[15] M. Liska, A. Al-Tabbaa, Performance of magnesia cements in porous blocks in acid and magnesium environments, Adv. Cem. Res. 24 (4) (2012) 221–232.
[16] Y. Li, J. Sun, B. Chen, Experimental study of magnesia and M/P ratio influencing properties of magnesium phosphate cement, Constr. Build. Mater. 65 (2014) 177–183.
[17] N.T. Dung, C. Unluer, Improving the performance of reactive MgO cement-based concrete mixes, Constr. Build. Mater. 126 (2016) 747–758.
[18] G. Cai, S. Liu, Y. Du, D. Zhang, X. Zheng, Strength and deformation characteristics of carbonated reactive magnesia treated silt soil, J. Cent. South Univ. 22 (5) (2015) 1859–1868.
[19] D. Wang, S. Di, X. Gao, R. Wang, Z. Chen, Strength properties and associated mechanisms of magnesium oxychloride cement-solidified urban river sludge, Constr. Build. Mater. 250 (2020).
[20] S. Liu, X. Zheng, G. Cai, J. Cao, Study of resistance to sulfate attack of carbonated reactive MgO-stabilized soils (In Chinese), Rock. Soil Mech. 37 (11) (2016) 3057–3064.
[21] G. Cai, S. Liu, X. Zheng, Influence of drying-wetting cycles on engineering properties of carbonated silt admixed with reactive MgO, Constr. Build. Mater. 204 (2019) (2019) 84–93.
[22] L. Wang, Experiment and technology research of carbonized composite pile based on permeable pipe pile, Master's Dissertation, Southeast Univ. (2019).
[23] S.-Y. Liu, G.-H. Cai, G.-Y. Du, L. Wang, J.-S. Li, X.-C. Qian, Field investigation of shallow soft-soil highway subgrade treated by mass carbonation technology, Can. Geotech. J. 58 (1) (2021) 97–113.
[24] G. Cai, Experimental and application studies on soft soils carbonated and stabilized by reactive magnesia, Ph. D. Diss., Southeast Univ. (2017).
[25] C. Qin, Experimental study on overall carbonization and solidification process of soft foundation, Master's Dissertation, Southeast Univ. (2019).
[26] GB/T 50123–2019, Standard for geotechnical testing method, China Planning Press, Beijing, 2019 (In Chinses).
[27] GB/T 50145–2007, Standard for engineering classification of soil, China Planning Press, Beijing, 2007 (In Chinese).
[28] YB/T 4019, Determination of chemical activity of light calcined magnesia Metallurgical Industry Press, Beijing, 2020 (In Chinses).
[29] G. Cai, S. Liu, G. Du, L. Wang, J. Li, L. Liu, Hydraulic conductivity characteristics of carbonated reactive magnesia-treated silt, Bull. Eng. Geol. Environ. 79 (2020) (2020) 3033–3047.
[30] P.J. Davies, B. Bubela, The transformation of nesquehonite into hydromagnesite, Chem. Geol. 12 (4) (1973) 289–300.
[31] S. Horpibulsuk, R. Rachan, A. Suddeepong, Assessment of strength development in blended cement admixed Bangkok clay, Constr. Build. Mater. 25 (4) (2011) 1521–1531.
[32] G. Cai, S. Liu, Y. Du, J. Cao, Influences of activity index on mechanical and microstructural characteristics of carbonated reactive magnesia-admixed silty soil, J. Mater. Civ. Eng. 29 (5) (2017) 12.
[33] C. Unluer, A. Al-Tabbaa, Enhancing the carbonation of MgO cement porous blocks through improved curing conditions, Cem. Concr. Res. 59 (2014) 55–65.
[34] S. Liu, G. Cai, J. Cao, F. Wang, Influence of soil type on strength and microstructure of carbonated reactive magnesia-treated soil, European, J. Environ. Civ. Eng. 24 (2) (2017) 248–266.
[35] S. Ruan, J. Qiu, Y. Weng, Y. Yang, E.-H. Yang, J. Chu, C. Unluer, The use of microbial induced carbonate precipitation in healing cracks within reactive magnesia cement-based blends, Cem. Concr. Res. 115 (2019) 176–188.